

https://dspace.org/

Optimal decarbonisation parthway for mining truck fleets

G Yu; X Ye; Yuxiang Ye; H Huang; X Xia

https://hdl.handle.net/10539/47352
SCOPUS

Downloaded from a DSpace repository. https://dspace.org/

Journal of Automation and Intelligence 3 (2024) 129–143

Contents lists available at ScienceDirect

Journal of Automation and Intelligence

journal homepage: www.keaipublishing.com/en/journals/journal-of-automation-and-intelligence/



Research article

Optimal decarbonisation pathway for mining truck fleets



Gang Yu [a], Xianming Ye [a,*], Yuxiang Ye [b], Hongxu Huang [c], Xiaohua Xia [a]

[a] Department of Electrical, Electronic and Computer Engineering, University of Pretoria, Pretoria 0002, South Africa
[b] School of Economics and Finance, University of the Witwatersrand, Johannesburg 2000, South Africa
[c] School of Information and Control Engineering, China University of Mining and Technology, Xuzhou 221116, China

ARTICLE INFO

Keywords:
Coal mine
Truck fleet
Carbon emission
Optimal decarbonisation pathway

ABSTRACT

The fossil fuel powered mining truck fleets can contribute up to 80% of total emissions in open pit mines. This study investigates the optimal decarbonisation pathway for mining truck fleets. Notably, our proposed pathway incorporates power generation, negative carbon technologies, and carbon trading. Technical, financial, and environmental models of decarbonisation technologies are established, capturing regional variations and time dynamic characteristics such as cost trends and carbon capture efficiency. The dynamic natures of characteristics pose challenges for using the cost-effective analyses approach to find the optimal decarbonisation pathway. To address this, we introduce a mixed-integer programming optimisation framework to find the decarbonisation pathway with minimum life cycle costs during the planning period. A case study for the optimal decarbonisation pathway of truck fleets in a South African coal mine is conducted to illustrate the applicability of the proposed model. Results indicate that the optimal decarbonisation pathway is significantly influenced by factors such as land cost, annual budget, and carbon trading prices. The proposed method provides invaluable guidance for transitioning towards a cleaner and more sustainable mining industry.

1. Introduction

The mining industry, responsible for 4%–7% of greenhouse gas (GHG) emissions globally, confronts multifaceted challenges posed by climate change [1]. The increased frequency and severity of extreme climate events damage the mining infrastructure. The warm winter in 2006 shortened the operation time of the ice road transportation network in northern Canada by nearly a month, forcing the Diavik diamond mine (owned by Rio Tinto) to change road transportation to air transportation by spending an extra $ 11.25 million [2]. Climate change intensifies the pollution caused by mining operations, including acid mine drainage, soil contamination, and the disruption of ecological systems, and exacerbates concerns about health hazards within the local community. For instance, the increased precipitation increases levels of water in pit lakes and tailings dams, thus contaminating surface water and shallow groundwater with minerals and mining wastes [3]. The heavy rainfall events lead to the infiltration of heavy metals, such as copper and arsenic, from uncontained tailings of copper mining into residential areas in Nacozari, Mexico [4]. The diminishing annual precipitation, attributed to global warming, escalates the persisting tensions between the mining industry and food and water security in Mpumalanga province of South Africa. The province has almost half of South Africa's high-potential arable land while over 60% of the province's surface area either being subject to mining rights or prospecting applications [5]. The challenges posed by climate change, as well as increasing stress from government, investors, and the public, force mining companies to transition to low-carbon and sustainable production patterns. The mining transportation fleet is one of the primary sources of on-site GHG emissions of the mining industry, which can account for up to 30% of on-site GHG emissions or up to 80% if the mine is without refinery facilities [6]. In [7], it is reported that mineral loading and hauling operations account for 41.4% of total energy consumption and contribute 37.1% of GHG emissions during coal mineral processing. Therefore, decarbonising the transportation system is critical for the decarbonisation of the whole mining production process.

This study explores the optimal decarbonisation pathway for mining truck fleets. The decarbonisation pathway is a step-by-step plan that outlines the necessary annual financial and technological investments to gradually decrease the carbon intensity of truck fleet activities, ultimately achieving the final decarbonisation goal [8]. Intuitively, the decarbonisation pathway has a start point and an end point. The start point involves the current fleet configurations and the corresponding energy consumption and carbon emissions, usually obtained through carbon accounting [9]. Meanwhile, the end point represents the desired fleet configurations with significantly reduced carbon emissions. The carbon emission target is expected to be consistent with the 1.5 °C

Peer review under responsibility of Chongqing University.
* Corresponding author.
E-mail address: xianming.ye@up.ac.za (X. Ye).

https://doi.org/10.1016/j.jai.2024.03.003
Received 15 December 2023; Received in revised form 14 February 2024; Accepted 15 March 2024
Available online 20 March 2024
2949-8554/© 2024 The Authors. Published by Elsevier B.V. on behalf of KeAi Communications Co. Ltd. This is an open access article under the CC BY-NC-ND license (http://creativecommons.org/licenses/by-nc-nd/4.0/).

and 2 °C targets of the Paris Agreement [10]. The pathway encompasses the measures required to traverse from the initial high carbon intensity fleet to the carbon-neutral or carbon-negative truck fleet, such as renewable energy integration, carbon capture, and carbon trading. The object is to create a clear and manageable framework for fleet stakeholders to understand what types of actions and investments are needed at what scale and by when in the future.

Early efforts in exploring the decarbonisation of truck fleets powered by fossil fuels focus on enhancing the energy efficiency of trucks, optimising logistical systems, and investigating alternative power sources. The enhancement of truck energy efficiency involves the improvement of aerodynamics, engine efficiency, transmission, drivetrain, etc [11]. For the logistical systems, energy efficiency is typically advanced by optimising transportation routes, waiting times, and fleet sizes, therefore reducing GHG emissions per unit production [12,13]. Optimising logistical systems is a cost-effective approach to achieving decarbonisation targets in the short term. The cost analysis in [12] demonstrates that incorporating smart dispatching into an existing fleet can yield 10%–30% reduction in emissions, and the associated adoption cost equates to 47% of fleet electrification costs. Nevertheless, it is imperative to acknowledge that while improvements in the energy efficiency of trucks and logistical systems can effectively mitigate emissions from truck fleets, achieving a fully zero-emission fleet remains elusive. For this purpose, alternative power sources for trucks are developed rapidly, whereas battery electric trucks (BETs) and hydrogen fuel cell trucks (HFCTs) are regarded as primary alternatives [14–16]. The life-cycle assessment conducted in [15] indicates that for Class 8 heavy-duty trucks, battery significantly outperformed other alternatives including compressed natural gas, biodiesel, and hybrid in terms of life-cycle costs and environmental impacts. If BETs are charged by the grid comprising about 10% coal, reductions on fuel consumption-related emissions and the life-cycle cost surpass 70% and 63%, respectively. Ref. [16] compares the life cycle GHG emissions from diesel, battery, and hydrogen fuel cell medium-duty urban delivery trucks in Singapore. The research indicates that BETs powered by the 2019 electricity mix have up to 11% lower GHG emissions than conventional diesel, but doubling battery capacity to meet travel range requirements results in up to 12% higher emissions. FCTs using gaseous hydrogen via steam methane reforming achieve 23%–30% GHG reductions. The optimal replacement strategy for trucks with alternative power sources is investigated in the literature to determine the purchasing and salvaging decisions for trucks and the construction plan of supporting infrastructures like charging stations and hydrogen refuelling stations to decarbonise transportation fleets. Ref. [17] proposes an integer linear program-based cost minimisation solution for bus fleet electrification while taking battery capacity and charger type into account. However, the authors ignore the changes in fuel and energy costs. In [18], a mixed-integer linear programming model is proposed to support the fleet replacement decision process for urban freight transport fleets while taking into account several types of electrified vans including battery electric vehicles, hydrogen fuel cell vehicles and range extender hybrid electric/hydrogen fuel cell vehicles and the energy supply infrastructure. In [19], the authors show a cost-minimising strategic green transition plan for truck fleets, and the congestion effect at the charging stations and the loss of time cost due to detours to reach charging stations are considered. In countries that heavily rely on fossil fuel power generation like China and South Africa, electrification of truck fleets will increase emissions if there is no green power generation assisted [20]. Therefore, the optimal decarbonisation pathway requires investments in green power generation, which is not considered in previous studies [17–19]. In addition, the adoption of alternative power sources, while crucial for mitigating future emissions, faces a critical limitation — it cannot address the historical emissions of the fleet. A just energy transition necessitates a comprehensive consideration of historical emissions and their profound influence on shaping decarbonisation pathway. Addressing historical emissions becomes integral in ensuring an equitable and balanced transition towards sustainable energy practices [21]. Within this context, the integration of carbon capture technologies promises an opportunity to substantially bolster decarbonisation efforts. These technologies offer the potential to address not only current emissions but also the historical emissions accumulated by truck fleets. Despite this potential, their incorporation remains insufficiently explored in ongoing research initiatives.

Carbon capture technologies are designed to remove CO_2 emissions produced by various sources before they enter the atmosphere. There are several types of carbon capture methods, including pre-combustion capture, post-combustion capture, oxy-fuel combustion, direct air capture (DAC), and biological carbon capture. The pre-combustion capture method operates on the principle of separating CO_2 from carbonaceous fuels such as coal or natural gas before the combustion process occurs. It converts fuels into hydrogen and carbon monoxide (known as syngas) by using a gasification process. The syngas are then processed to separate the carbon from the hydrogen and other components and obtain pure hydrogen gas for combustion [22]. The post-combustion capture method separates and captures CO_2 from other gases produced in the combustion process, such as in flue gas from power plants or industrial facilities. To date, post-combustion capture is recognised as the most established carbon capture strategy with proven pilot projects and commercial-scale plants such as Nanko Power Station in Osaka, Japan [23] and Statoil's Sleipner natural gas processing facility, Norway [24]. The results in [25] reveal that the net efficiency (the percent of net output of the plant compared with the fuel's calorific value) of coal-fired power plants using carbon capture and storage is about 10% lower than that of power plants without carbon capture and storage. The oxy-fuel combustion involves burning fuels in oxygen instead of air, creating a concentrated CO_2 stream that is easier to capture. The biological carbon capture technology includes forestation and microalgae and so on. Forestation involves planting trees to capture CO_2 from the atmosphere through photosynthesis and storing carbon within forests. The storing carbon can be categorised into above-ground carbon and below-ground carbon. The above-ground carbon refers to the carbon stored in tree trunks, branches, leaves, and other visible parts of the plant [26]. Below-ground carbon involves the carbon stored in roots, soil organic matter, and microbial communities associated with plant roots [27]. Through the carbon sequestration process, the carbon is transferred from plant roots into the soil, where it can remain stored for extended periods, contributing to below-ground carbon reservoirs [28]. The costs of forest carbon sinks exhibit significant regional variations. An analysis from [29] shows the carbon sink costs in China's 32 provinces vary from 16.7 $/ton to 1262.7 $/ton, depending on factors such as land availability, climate conditions, rotation period, and afforestation costs. The latest evaluation of the global forest carbon sink potential indicates a total of 328 Gt [30]. Within this estimate, the carbon sink potential within existing forests is 139 Gt, achievable through forest conservation practices to facilitate their recovery to mature states. Additionally, there is a carbon sink potential of 189 Gt in converted lands (areas where forests have been removed). This potential can be harnessed by converting farmland and grazing land back into forests, contingent upon the land-use decisions of local communities. Microalgae is one of the simplest and most ancient of the photosynthetic plants that grow in the aquatic system. Although microalgae reside in aqueous environments, the efficiency of microalgae using solar energy to fix carbon dioxide is 10–50 times higher than that of other terrestrial plants [31]. In addition, microalgae can multiply in a few hours, much higher than terrestrial plants, and has strong environmental adaptability. Identifying microalgae strains that exhibit robust traits such as high tolerance to CO_2 concentrations (exceeding 20%), efficient CO_2 fixation rates, and resilience to toxic compounds like NOx, SOx, and H_2S is crucial for scaling up microalgae-based carbon capture applications [32]. Certain strains like *Chlorella* and *Chlorococcum* [33] demonstrate effectiveness in capturing CO_2 from both industrial emissions and effluents. The DAC uses a combination of chemical processes

to capture CO_2 directly from the atmosphere, which is independent of CO_2 emission origin and can be deployed anywhere. Sorption DAC emerges as the primary technical route for the development of DAC comprehensively considering their advantages and disadvantages of energy penalty, stability, and cost [34]. In the sorption process, ambient air passes through the adsorbent, where the contained CO_2 is removed selectively. Then, the adsorbed CO_2 is released in a concentrated stream for further utilisation, while the adsorbent is regenerated, and CO_2-lean air returns to the atmosphere [35]. The selection of sorbents poses the main challenge to the development of DAC. It requires robust chemical stability and sustained sorption performance even after undergoing thousands of loading and unloading cycles [36]. Moreover, the low CO_2 concentration in the atmosphere requires large loading sorbents and high energy demand in the regeneration process, which lead to the costs of DAC are expected to be considerably higher than the discussed CO_2 capturing alternatives. Two groups of sorbents can be identified as most promising, from a technical and economic perspective. The first is based on using water solutions containing hydroxide sorbents with a strong affinity for CO_2, such as sodium hydroxide, calcium hydroxide, and potassium hydroxide. The second uses amine materials bonded to a porous solid support [37]. A wider range of solid sorbents are being investigated (e.g. ionic membranes, zeolites, solid oxides), but are still at the research stage.

This study investigates the optimal decarbonisation pathway for mine truck fleets, minimising the life cycle cost (LCCs) during the planning period. The identified decarbonisation technologies encompass alternative power sources for trucks, renewable energy power generation, carbon capture technology, and carbon trading. Considering the dynamic characterise of cost trends and carbon capture efficiency of decarbonisation technologies, an optimisation framework is introduced for the optimal decarbonisation problem. The decision variables are the type and scale of decarbonisation strategies invested each year. The investment budget of each year, capacity limitations, and the decarbonisation target constrain this problem. Compared to existing research, the contribution of this study is summarised as follows:

- The proposed optimal decarbonisation pathway considers renewable energy power generation, carbon trading, and carbon capture technologies, including forestation, microalgae, and direct air capture.
- Technical, financial, and environmental performances of decarbonisation strategies are modelled. The established models capture regional variations and dynamic characteristics such as cost trends and carbon capture efficiency.
- Considering the dynamic characteristics of truck fleets and decarbonisation technologies, a mixed integer programming model is established to seek the optimal decarbonisation pathway of the mining truck fleet.

The rest of this study is organised as follows. Section 2 details the methodology to find the optimal decarbonisation pathway for mining truck fleets. Section 3 proposes the energy consumption and carbon emission models for truck fleets and technical, financial, and environmental models for decarbonisation technologies. An optimisation framework is formulated in Section 4 to explore the optimal decarbonisation pathway with minimum LCCs. A case study is presented in Section 5. Section 6 concludes this study.

2. Methodology

The methodology to obtain the optimal decarbonisation pathway for the mining truck fleet is described in Fig. 1. The detailed steps are as follows:

Step 1: Determine the decarbonisation target. Generally, two key time nodes including years achieving zero carbon emission and cumulative carbon emissions are considered when formulating the decarbonisation target. Annual net carbon emissions (carbon neutrality) refer to the total amount of CO_2 emitted each year by a region or industry, calculated from the difference between annual carbon emissions and annual carbon emission reduction [38]. The next step after achieving carbon neutrality is to achieve zero cumulative carbon emissions, thereby making up for all CO_2 ever emitted. This target is proposed in [39]. The cumulative carbon emission is defined as the sum of CO_2 emitted since the base year. According to the GHG Protocol Corporate Standard [9], the base year is a year for which verifiable carbon emissions data are available. In this study, we assume that the base year for the truck fleet is 2023.

Step 2: Collect data. Related data includes weather data, energy price data, equipment parameters, and emission factors. The weather data includes the global horizontal irradiance (GHI), the photosynthetically active radiation (PAR), temperature, and wind speed of the location of the coal mine. The energy price data includes the price of diesel, grid electricity, green hydrogen, PV, wind turbines, trucks, carbon capture technologies, and carbon trading. The equipment parameters include fuel economy factors of trucks with different power sources, the annual mileage of trucks, and the number of trucks in the fleet. The emission factors of diesel, grid electricity, and hydrogen are required.

Step 3: Model the annual energy consumption and carbon emission of the mining truck fleet. This study involves Scope 1 and Scope 2 carbon emissions defined in the GHG Protocol Corporate Standard [9]. It divides an organisation's emissions into three scopes. Scope 1 includes emissions that result from activities within the mine transportation fleet's control. Scope 2 is the indirect emissions from the electricity that the fleet owners purchase and use. Scope 3 emissions are indirect emissions along the entire value chain attributable to the truck fleet and are not within the direct control of the mining truck fleet's operation. The reduction of Scope 3 emissions necessitates adjustments to the coal supply chain and changes in the behaviour of coal consumers [40]. However, as these emissions are not directly related to the day-to-day operation of the mining truck fleets, they are not included in the scope of this study.

Step 4: Evaluate the technical, financial, and environmental performances of decarbonisation technologies, including renewable energy (solar and wind energy) and negative carbon technology (forestation, microalgae, and DAC).

Step 5: Establish an optimisation framework to obtain the optimal investment schedule for various decarbonisation technologies. The objective function aims to minimise the LCC of the truck fleet throughout the planning duration, considering investment cost, O&M cost, land cost, grid electricity cost, carbon trading cost, and carbon tax. The optimisation problem is constrained by the decarbonisation target, annual budget, required annual productivity, etc.

Step 6: Analyse the obtained optimal decarbonisation pathway in terms of carbon emission and cost.

3. Modelling of decarbonisation strategies

This section models the annual energy consumption and carbon emission of trucks, the technical, financial, and environmental performance of renewable energy and negative carbon technology, and carbon trading, using a coal mine in South Africa as an example. Due to different raw material costs, labour costs, and climate conditions, these performances differ across countries, but the evaluation methodology is general.

3.1. Energy consumption and carbon emission modelling of trucks

This section models the annual energy consumption and carbon emissions of the truck fleet. As mentioned before, this study focuses on Scopes 1 and 2 emissions. All carbon emissions of the truck fleet are from energy consumption including fuel combustion and electricity consumption. Generally, the energy consumption of trucks can be

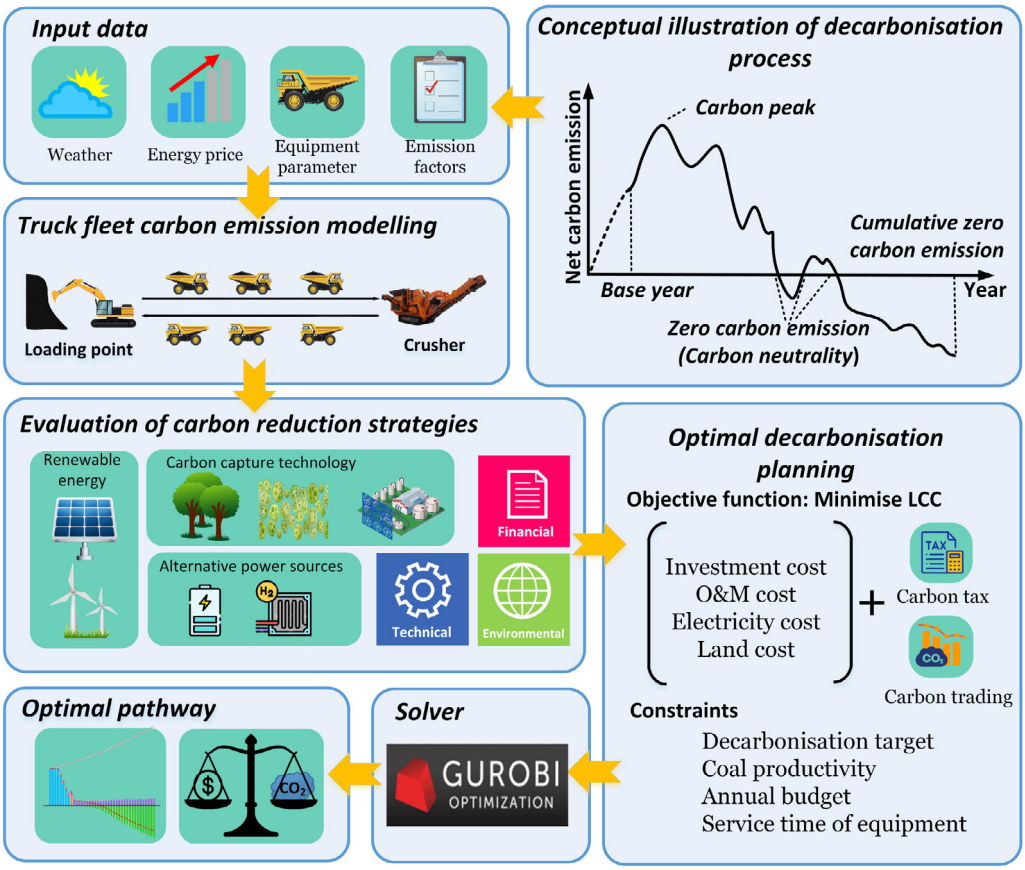


Fig. 1. Methodology of this research.

obtained through the fuel economy factor [41] or the vehicle dynamic model [42]. The fuel economy factor approach calculates the annual energy consumption of the fleet based on the annual mileage and corresponding fuel economy factors. The fuel economy factors vary in terms of types of trucks and usage scenarios. The vehicle dynamic model approach calculates energy consumption based on real-time operation parameters including vehicle speed, payload, and road condition [42]. The vehicle dynamic model approach is believed to have higher accuracy than the fuel economy approach but relies on massive real-time operational data. In contrast, the fuel economy approach only used fewer data (typically annual mileage) for calculation. Therefore, this study adopts the fuel economy approach to calculate energy consumption and carbon emissions. Denote a set $\mathcal{V} = \{\text{di(esel)}, \text{ba(ttery)}, \text{hy(drogen)}\}$. The annual energy consumption of one truck is calculated by

$$F_v = Mq_v, v \in \mathcal{V}, \tag{1}$$

where M is the annual mileage of one truck and q_v is the fuel economy of trucks with different power sources. The annual carbon emission of one truck is calculated by

$$E_v^{mt} = F_v z_v, v \in \mathcal{V}, \tag{2}$$

where $z_v, v \in \mathcal{V}$ represent the emission factors of diesel, electricity, and hydrogen. The values of q_v and z_v are given in Table 1.

Table 1
Fuel economy and emission factors for diesel trucks, BETs, and HFCTs.

	Diesel	Battery	Hydrogen
Fuel economy	15.6 litre/km	55.6 kWh/km	3.7 kg/km
Emission factor	2.7 kg CO_2/litre	0.99 kg CO_2/kWh	0 kg CO_2/kg

In practice, the annual mileage of trucks M is easily obtained from the truck's dashboard. However, this data is not available in this study, thus we have to use analytical methods. Intuitively, the annual mileage is related to the annual coal handling demand G, the capacity of the truck fleet, and the distance between load and dump points D. Then, the annual mileage of one truck is estimated as

$$M = \frac{2GD}{NC}, \tag{3}$$

where N is the number of trucks in the fleet and C represents the tramming capacity of one truck. The proposed model examines the relationship between energy consumption and annual mileage, incorporating two key parameters: fuel economy factors and truck annual mileage. It is essential to recognise that unmodelled dynamics, such as load weight, idling, and terrain characteristics, introduce uncertainties. These uncertainties are addressed by converting them into variations in the values of fuel economy factors. The development of fuel economy factors exceeds the scope of this study, refer to related research for more details [43]. Consequently, we adopt the results in [7,44], derived from actual coal mine operation data.

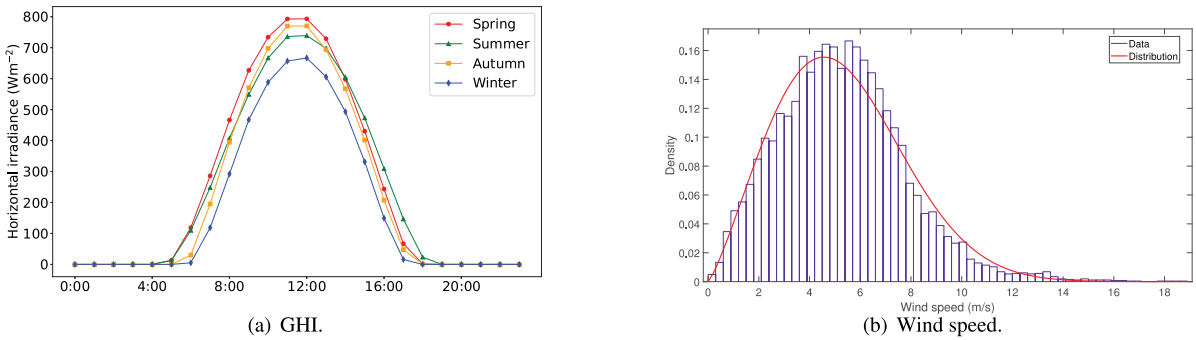
In the case study, sensitivity analysis is conducted to investigate the impact of annual mileage uncertainty on the optimal decarbonisation pathway.

3.2. Modelling of PV and wind energy power generation

The annual power generation of PV system is given by

$$W_0 = \eta_{pv} H_{si} A_{pv}, \tag{4}$$

where H_{si} is the annual total solar irradiation on the PV array in kWh·m^{-2}, η_{pv} is the panel efficiency, and A_{pv} is the installed area of



(a) GHI. (b) Wind speed.

Fig. 2. The GHI and wind speed in the region of interest.

the PV system. The production energy of PV systems is affected by degradation. Let d_{pv} be the degradation factor, the energy generated by solar panels of age j is given by

$$W_j^{pv} = W_0(1 - d_{pv})^{j-1}. \tag{5}$$

The power output of one wind turbine is calculated as

$$P^{wd} = \begin{cases} \frac{1}{2}\rho A_b \bar{v}^3, v_{cin} < \bar{v} < v_r, \\ \frac{1}{2}\rho A_b v_r^3, v_r < \bar{v} < v_{cou}, \\ 0, \text{ otherwise }, \end{cases} \tag{6}$$

where $\bar{v}$, v_r, v_{cin}, v_{cou} are instantaneous, rated, cut-in and cut-out wind speeds, respectively (in $\mathrm{m{\cdot}s^{-1}}$). A_b is the swept area of the blades. Assume $\bar{v}$ following a distribution $f_{wd}(\bar{v})$, the wind power production is given by

$$D_{wd} = \int P^{wd}(\bar{v}) f_{wd}(\bar{v}) \mathrm{d}\bar{v}. \tag{7}$$

Similar to the PV system, let d_{wd} be the degradation factor of wind turbines, the energy generated by one wind turbine of age j is given by

$$W_j^{wd} = 8760 D_{wd}(1 - d_{wd})^{j-1}. \tag{8}$$

The solar irradiance and wind speed of the location of the coal mine can be obtained from NASA's POWER Project [45]. The climate data from 2020/01/01 to 2020/12/31 including hourly average GHI and wind speed are shown in Fig. 2. Then, we can calculate $H_{si} = 1972\ \mathrm{kWh{\cdot}m^{-2}}$. The efficiency of solar panels is highly related to the materials of the panels. IEA's report reveals that crystalline polysilicon remains the dominant technology for PV modules, with over 95% market share [46]. Therefore, the crystalline polysilicon panel is adopted in this study. The efficiency is 19%–22% [47]. In this study, $\eta = 22\%$. The degradation factor is 0.7% [48]. The wind speed follows the Weibull distribution with $k = 2.23, c = 5.95$, obtained by Matlab Distribution Fitter Toolbox. According to the review in [49], the v_r, v_{cin}, v_{cout} are selected as 4 $\mathrm{m{\cdot}s^{-1}}$, 13.5 $\mathrm{m{\cdot}s^{-1}}$, and 25 $\mathrm{m{\cdot}s^{-1}}$. The O&M costs for PV and onshore wind energy are 5% of their installation costs [50]. The useful lifespan is 20 years.

The learning curve approach is widely employed in technology and innovation to forecast the cost reduction of new products as more units of a product are manufactured [51]. In this study, it is used to calculate the installation cost for PV and wind turbines. The learning curve model is given as follows

$$c_t = c_{t_0}\left(\frac{q_t}{q_{t_0}}\right)^{\frac{\ln(1-LR)}{\ln 2}}, \tag{9}$$

where c_t represents the installed costs of PV and onshore wind energy in year t, and q_t represents the total installed capacities of PV and onshore wind energy. LR is the learning rate. According to [52], the learning rates over the last 40 years are around 20% for solar PV, and 10% for wind energy, respectively. The global average installed costs for renewable energy for 2022 are sourced from the International Renewable Energy Agency (IRENA) [53], 876 $/kW for solar PV and 1274 $/kW for onshore wind, respectively. The historical installation capacities from 2013 to 2022 for PV and onshore wind energy are obtained from [54]. Linear and quadratic function models are used to fit the growth trends of PV and onshore wind energy installed capacity, respectively, as shown in Fig. 3. The installed capacities from 2023 to 2050 for PV and onshore wind energy are obtained based on their trend lines. Then, the installation cost for PV and onshore wind energy can be obtained according to (9). The results are summarised in Fig. 4.

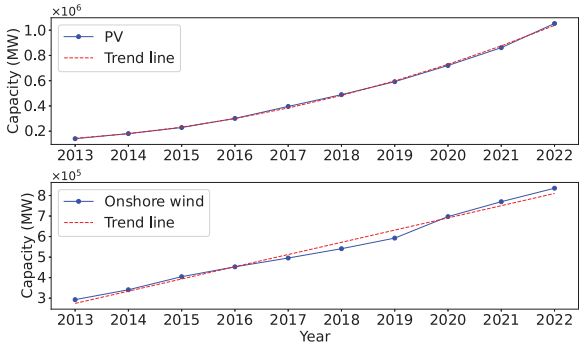


Fig. 3. Global PV and onshore installed capacity from 2013 to 2022.

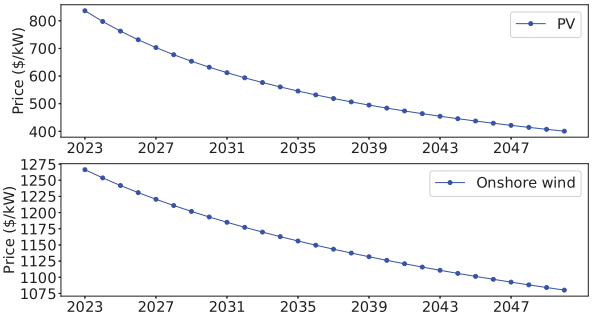


Fig. 4. Global PV and onshore installed cost forecasting from 2023 to 2050.

3.3. Modelling of negative carbon technology

3.3.1. Forestation

According to [55], the increase in total carbon stock including both above- and below-ground carbon following forestation (ton per hectare) is given by

$$\bar{E}_j^f = 0.00025j^3 - 0.05835j^2 + 5.815j, \tag{10}$$

where j is the age of the forest. Then, the annual capture amount by the forest can be calculated as

$$E_j^f = \begin{cases} \frac{44}{12}\bar{E}_j^f, & j = 1, \\ \frac{44}{12}(\bar{E}_{j+1}^f - \bar{E}_j^f), & j \geq 2. \end{cases} \tag{11}$$

According to [56], the forestation cost is $ 5774.86 per hectare.

3.3.2. Microalgae cultivation

The regulation of microalgal growth hinges upon crucial parameters such as temperature, nutrient concentration, light intensity, CO_2 and O_2 concentrations, pH, and salinity [57]. Literature contributes extensively by developing growth kinetic models that account for single and multiple influencing factors, see reviews in [58]. In the context of outdoor cultivation, temperature and light intensity emerge as paramount regulators governing microalgal growth and exhibit substantial regional variations [59]. Recognising this, kinetic models tailored to these two factors are used in this study to adapt to the specific requirements of mines in different areas [60,61]. The growth kinetic model of microalgae in an open pond is given as

$$\frac{dC_b}{dt} = \frac{\phi_L(t)\phi_T(t) * PAR(t) * \phi_{photon}A_c}{V} + \frac{R(t)}{V}, \tag{12}$$

where C_b is the concentration of biomass in g·m^{-3}, V is the volume in m^3, $R(t)$ is the respiratory decay rate in g·s^{-1}, $\phi_{photon} = 1.5$ g·mol^{-1} represents the photon efficiency, $PAR(t)$ is the rate of photosynthetic spectrum photon incidence (in μmol·m^{-2}·s^{-1}), which represents the spectral range of solar radiation from 400 to 700 nm that photosynthetic organisms can use in the process of photosynthesis. Generally, the ratio of PAR to GHI is between 0.41–0.57 across locations in South Africa [62] (1 μmol·m^{-2}·s^{-1} = 4.57 W·m^{-2}). A_c is the culture area in m^2, while $\phi_L(t)$ and $\phi_T(t)$ represent dimensionless efficiency factors dependent on the incident light intensity, and reactor temperature, respectively. The average light intensity is given by

$$I_{ave} = \frac{1}{A_d}\int_0^{A_d} GHIe^{-K_e s}ds, \tag{13}$$

where A_d is the pond depth in metres, and K_e is the extinction coefficient of the microalgae culture. In [63], $K_e = 0.32 + 0.03C_b$. Then, the light efficiency is given by

$$\phi_L = \frac{I_{avg}}{I_{sat}}\exp\left(1 - \frac{I_{avg}}{I_{sat}}\right), \tag{14}$$

where I_{sat} represents the saturation light intensity in W·m^{-2}.

The temperature efficiency is modelled by

$$\phi_T = \frac{(T_w(t) - T_{\max})(T_w(t) - T_{\min})^2}{(T_{opt} - T_{\min})[g_1(T_w(t)) - g_2(T_w(t))]}, \tag{15}$$

$$g_1(T_w(t)) = (T_{opt} - T_{\min})(T_w(t) - T_{opt}), \tag{16}$$

$$g_2(T_w(t)) = (T_{opt} - T_{\max})(T_{opt} + T_{\min} - 2T_w(t)), \tag{17}$$

where $T_w(t)$ is the water temperature, and T_{min}, T_{max}, and T_{opt} are the minimum, maximum, and optimal temperatures for the cultured microalgae, respectively.

The respiratory loss decay rate is given by

$$R(t) = \begin{cases} C_b\frac{\ln(1-\kappa)}{3600\Delta t}V\phi_T(t), & \text{if } GHI \geq 5, \\ 0, & \text{if } GHI < 5, \end{cases} \tag{18}$$

Table 2
Parameters of microalgae production model [60,61].

Parameters	Values	Units
Saturation light intensity I_{sat}	294.12	μmol·m^{-2}·s^{-1}
Maximum temperature $T_{\max}$	42	°C
Minimum temperature $T_{\min}$	5	°C
Optimal temperature T_{opt}	27	°C
Dark loss κ	4.5	% AFDW
Depth of the pond A_d	2	m
Area of the pond A_c	1	m^2

where κ represents the biomass loss [% AFDW] over the entire dark period, and Δt is the length of the dark period in hours.

The thermal model of an open pond is given by

$$\rho C_s V\frac{dT_w}{dt} = \sum Q_i, \tag{19}$$

where ρ represents the culture density, C_s is the culture-specific heat in J·kg^{-1}·K^{-1}, and $\sum Q_i$ is the sum of all relevant heat fluxes, including Q_{sol}, Q_{air}, Q_{gro}, Q_{rad}, Q_{con}, Q_{eva}, and Q_{inf}. They are defined as follows.

The heat transfer due to direct irradiance of the open raceway pond surface is given by

$$Q_{sol} = (1 - f_s)GHIa_{culture}A_c, \tag{20}$$

where $f_s = 0.025$ represents the fraction of sunlight converted into chemical energy by the microalgae during photosynthesis, and $a_{culture} = 0.82$ denotes the absorptivity of microalgae culture.

The air radiation heat flux is

$$Q_{air} = \kappa_w\kappa_a\sigma T_a^4 A_c, \tag{21}$$

where $\kappa_w = 0.97$ and $\kappa_a = 0.85$ are the emissivities of the microalgae and water mixture and air, respectively. σ is the Stephan-Boltzmann constant. T_a is the ambient temperature.

The ground conduction heat flux

$$Q_{gro} = -\epsilon_t\frac{(T_w - 290)}{A_d}A_c, \tag{22}$$

where $\epsilon_t = 1.4$ is the thermal conductivity of concrete.

The pond radiation heat flux

$$Q_{rad} = -\sigma\kappa_w T_a^4 A_c. \tag{23}$$

The convection at the pond surface is given by

$$Q_{con} = \theta_c(T_a - T_w)A_c, \tag{24}$$

where θ_c is the convection coefficient.

The evaporation and evaporative cooling heat flux is modelled as

$$Q_{eva} = -\epsilon_e l_w A_c, \tag{25}$$

where ϵ_e is the evaporation rate in kg·m^{-2}·s^{-1}. For the determination of ϵ_e and θ_c, please refer [64]. $l_w = 2.45 \times 10^6$ J·kg^{-1} is the latent heat of water.

The inflow heat flux is

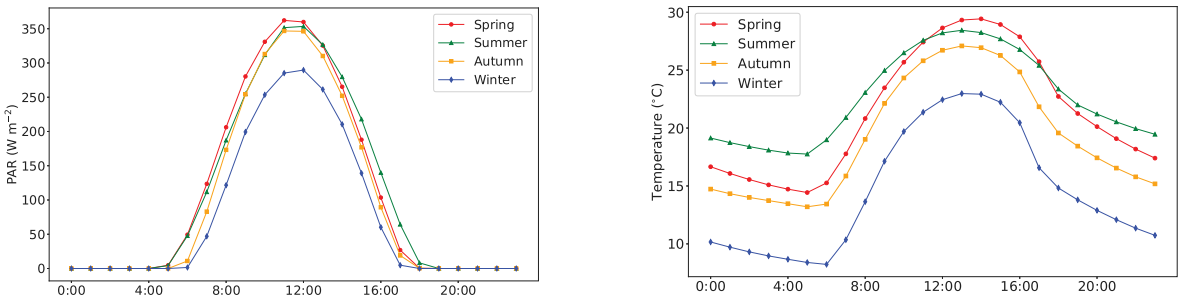
$$Q_{inf} = C_p\epsilon_e(T_a - T_w), \tag{26}$$

where $C_p = 4184$ J·kg^{-1}·K^{-1} is the specific heat capacity of the microalgae slurry.

The model parameters are given in Table 2. The temperature and PAR data can be obtained from NASA's POWER Project [45], shown in Fig. 5. Then, the microalgae productivity per m^2 per day is calculated as 13.82 g in Spring, 13.97 g in Summer, 12.24 g in Autumn, and 7.72 g in Winter.

The annual amount of CO_2 absorbed by 1 m^2 microalgae in an open pond (kg·year^{-1}) is estimated as

$$E_a = 365\frac{44}{12}\Delta C_b C_c, \tag{27}$$



(a) PAR. (b) Temperature.

Fig. 5. The PAR and temperature in the region of interest.

where ΔC_b is the average daily productivity of microalgae per m^2, C_c is the carbon content ratio in microalgae. According to the equivalent chemical formula of microalgae $CO_{0.48}H_{1.83}N_{0.11}P_{0.11}$, C_c is calculated as 45.35 wt%.

The main capital costs of open raceways include the cost of paddlewheels, liners for the pond as well as pond covers. The water consumption of algae cultivation ranged from 4.59 $m^3 \cdot m^{-2} \cdot year^{-1}$ in a tropical climate to 6.39 $m^3 \cdot m^{-2} \cdot year^{-1}$ in an arid climate, which constitutes a relatively minor portion of the overall operational costs [65,66]. The costs of nutrients, maintenance, harvesting, and dewatering costs are the major contributors to the operation costs. According to the calculation in [66], the capital cost and operating costs for microalgae cultivation in open raceway ponds are 0.7959 \$/m^2 and 2.4745 \$/m^2, respectively. The learning rate of algae is 12.4% [67]. The historic global algae production data from 1950 to 2019 is obtained from [68] as shown in Fig. 6. The global algae production forecasting from 2024 to 2050 is based on the trend line, where the quadratic function is employed to fix the historic global algae production data. The capital cost and operation cost of algae cultivation are shown in Fig. 6.

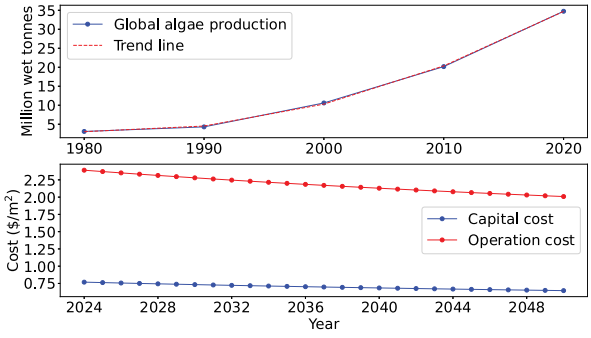


Fig. 6. Cost of microalgae cultivation.

3.3.3. Direct air capture

This section models the solvent-based DAC systems. During the operation of solvent-based DAC systems, 80% of the required energy is in the form of high-temperature thermal energy (largely for calcination) and 20% of the required energy is electricity (largely for compressors, pumps, and fans). The utilisation of both electricity and natural gas contributes to the main operational costs. Since there is no reliable data source for the historical price of natural gas, a variant outlined in [69] is considered: DAC powered by fossil-fuel-free electricity, using electric resistance heating to meet thermal energy needs. When operating with grid-powered electricity, the total operation cost of capturing 1 ton CO_2 is calculated as

$$c_{dac}^{ope} = p_{grid} W_e^{dac} + rc_{dac}^{cap}, \tag{28}$$

where W_e^{dac} are the electricity consumed when capturing 1 t CO_2. rc_{dac}^{cap} represents the cost of maintenance, labour, and chemical consumption. Considering the emission of grid electricity, the net amount of CO_2 captured is calculated by

$$E_{dac} = 1 - e_{grid} W_e^{dac}. \tag{29}$$

When the DAC is powered by the green power generation, $E_{dac} = 0$ ton. According to [69], the capital cost of DAC is 2027 \$/ton including contactor, air contactor, regeneration system, and compressor, and W_e^{dac} = 2628 kWh/ton. Estimating future DAC cost requires three fundamental input datasets: (1) The initial DAC cost; (2) The historic and future cumulative DAC capacity demand; and (3) The learning rates for DAC systems. In this study, the prediction of DAC capacity is obtained from IEA's report [70]. Since the global deployment of DAC is still in its early stages, the learning rate is 15% based on the estimation in [71], which is experienced from comparable technologies including water electrolysers (18%), seawater reverse osmosis desalination (15%, lithium-ion battery systems (12%–17%).

3.4. Carbon trading

The carbon trading system builds a ready market for carbon permits helping companies to trade so that they can meet their allocated emission limit. At the end of each year, each company is required to ensure they have enough carbon permits to cover their emissions. Companies have the flexibility to purchase additional carbon permits from the market. Those companies with carbon permits left over can sell them or save them for future use.

Although the carbon trading system has not been established yet in South Africa, the impact of the carbon trading system can be investigated by referring to other countries' carbon trading prices. Currently, the carbon trading price varies a lot in different countries. According to the World Bank's data [72], this study roughly categorises countries/regions into three types in terms of carbon prices, namely countries/regions with low carbon prices, middle carbon prices, and high carbon prices. As shown in Table 3, China, Regional Greenhouse Gas Initiative (RGGI, United States), and Korea are countries with low carbon prices, the carbon prices vary from \$ 8.15–\$ 15.39 in 2023. Austria, Canada, and New Zealand are countries with middle carbon prices. The carbon prices vary from \$ 34.2–\$ 48.03 in 2023. European Union (EU), United Kingdom (UK), and Switzerland have the highest carbon prices. The carbon prices vary from \$ 88.13–\$ 96.3 in 2023. This study selects RGGI, New Zealand, and the EU as references for carbon prices. The historical carbon trading prices and fitting trendlines of the three countries/regions are shown in Fig. 7. The fitting results are given in Table 3.

Table 3
Carbon prices in different countries.

Scenario	Representative country	Price in 2023 ($/ton)	Trendline of carbon price	R^2
Low price	China, **RGGI**, Korea	8.15–15.39	$c_i^{ct} = 1.6981i^2 - 11.813i + 22.185$	0.9469
Middle price	Austria, Canada, **New Zealand**	34.2–48.03	$c_i^{ct} = 1.3807i^{1.3548}$	0.9257
High price	**EU**, UK, Switzerland	88.13–96.3	$c_i^{ct} = 0.2282i^2 - 1.7684i + 6.9499$	0.8794

*Trend lines correspond to countries using bold.

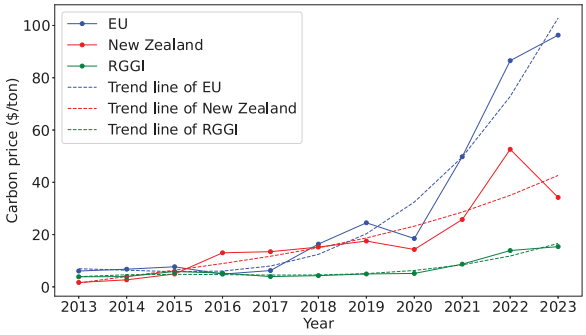


Fig. 7. Carbon prices in EU, RGGI, and New Zealand from 2013 to 2023.

4. Optimisation problem formulation

The previous section presents technical, financial, and environmental models of decarbonisation technologies. Importantly, these models are able to capture regional variations and dynamic characteristics such as cost trends and carbon capture efficiency. In addition, other dynamic parameters like energy and fuel costs influence the optimal decision. The dynamic nature of these aspects complicates the identification of an optimal decarbonisation pathway through the cost-effective analysis approach used in [73]. To address this, we propose a mixed-integer programming optimisation based framework designed to optimise the decarbonisation pathway.

The objective function aims to minimise the LCC of decarbonisation strategies across K_h years. To enable the formulation, we define sets $\mathcal{I} = \{\text{pv}, \text{wi(nd)}, \text{fo(restation)}, \text{mi(croalgae)}, \text{da(c)}\}$ and $\mathcal{V} = \{\text{di(esel)}, \text{ba(ttery)}, \text{hy(drogen)}\}$.

$$\min \text{LCC} = \sum_{k=1}^{K_h} \frac{1}{(1+r)^k} \left(\sum_{i}^{\mathcal{I}} \sum_{j=1}^{s_i} c_{i,j}^{\mathcal{I},k} X_{i,j}^k + \sum_{v}^{\mathcal{V}} \sum_{j=1}^{s_v} c_{v,j}^{\mathcal{V},k} Y_{v,j}^k + \sum_{i}^{\mathcal{I}} \sum_{j=1}^{s_i} l_i X_{i,j}^k + c_{ct}^k E_{ct}^k + c_{tax}^k \max\{E^k, 0\} + c_{grid}^k X_{grid}^k - \sum_{i}^{\mathcal{I}} \sum_{j=1}^{s_i} q_i^{\mathcal{I}} S_{i,j}^{\mathcal{I},k} - \sum_{v}^{\mathcal{V}} \sum_{j=1}^{s_v} q_v^{\mathcal{V}} S_{v,j}^{\mathcal{V},k} \right). \tag{30}$$

The objective function (30) contains six parts: investment and operation costs of carbon reduction technologies and trucks, land rent costs, carbon trading costs, carbon tax, electricity costs, and salvage values of decarbonisation technologies and trucks. The implementation of renewable energy power generation and negative carbon technologies demands a substantial amount of land, potentially exceeding the available land area within the mines. To address this, we incorporate the land rent cost into the objective function, which enables mines to lease extra land for the deployment of renewable energy power generation and negative carbon technologies. l_i is the land use factor. r is the discount rate. $X_{i,j}^k$, $Y_{v,j}^k$, E_{ct}^k, E^k, X_{grid}^k, $S_{i,j}^{\mathcal{I},k}$ and $S_{v,j}^{\mathcal{V},k}$ are decision variables, $i \in \mathcal{I}$, $v \in \mathcal{V}$. $X_{i,j}^k$ is a continuous variable that represents the installed capacity of ith technology with age j in year k. $Y_{v,j}^k$ is an integer variable that represents the number of purchased vth type vehicles with age j in the fleet in year k. E_{ct}^k is the amount of carbon sink brought from the carbon trading market in year k. E^k is the net emission of the mining truck fleet in year k. X_{grid}^k is the amount of purchased electricity from the grid in year k. $S_{i,j}^{\mathcal{I},k}$ and $S_{v,j}^{\mathcal{V},k}$ are continuous variables and integer variables that represent the retired capacity of ith technology with age j in year k and numbers of vth type of vehicles with age j. $c_{i,j}^{\mathcal{I},k}$ and $c_{v,j}^{\mathcal{V},k}$ are the unit investment or operation cost of ith type of technology and vth type of truck with age j in year k. c_{ct}^k is the carbon trading price in year k. c_{tax}^k is the carbon tax rate in year k. c_{grid}^k is the price of electricity brought from the grid. s_i and s_v represent the useful lifespans of ith type of technology and vth type of trucks, respectively. $q_i^{\mathcal{I}}$ and $q_v^{\mathcal{V}}$ are the salvage value of ith type of technology and vth type of trucks, respectively. There is a nonlinear term $\max\{E^k, 0\}$ in the objective function. It can be linearised by introducing a new continuous decision variable $u^k = \max\{E^k, 0\}$. u^k satisfies

$$u^k \geq E^k, \tag{31}$$

$$u^k \geq 0. \tag{32}$$

The following constraints are satisfied

$$X_{i,j}^k = X_{i,j-1}^{k-1} - S_{i,j}^{\mathcal{I},k}, j = 2, \ldots, s_i, \tag{33}$$

$$Y_{v,j}^k = Y_{v,j-1}^{k-1} - S_{v,j}^{\mathcal{V},k}, j = 2, \ldots, s_v, \tag{34}$$

$$S_{i,j}^{\mathcal{I},k} \leq X_{i,j-1}^{k-1}, j = 2, \ldots, s_i, \tag{35}$$

$$S_{v,j}^{\mathcal{V},k} \leq Y_{v,j-1}^{k-1}, j = 2, \ldots, s_v, \tag{36}$$

$$S_{i,1}^{\mathcal{I},k} = 0, S_{v,1}^{\mathcal{V},k} = 0, \tag{37}$$

$$S_{i,j}^{\mathcal{I},1} = 0, S_{v,j}^{\mathcal{V},1} = 0, \tag{38}$$

$$\sum_{v}^{\mathcal{V}} \sum_{j=1}^{s_v} Y_{v,j}^k = N. \tag{39}$$

Constraints (33) and (34) are capacity/quantity balance equations for each type of technology i and vehicle v, respectively. Constraints (35) and (36) indicate that the retired capacity/number of technology i and vehicle with age j in year k should be less or equal to the installed capacity/number. Both technology i and vehicle v will be retired when achieve their useful lifespans. Constraint (37) and (38) are used to ensure that the invested technologies and vehicles are not retired in the first year. Constraint (39) ensures the total number of trucks in the fleet equals N.

$$X_{i,j}^k = 0, j \geq s_i + 1, \tag{40}$$

$$Y_{v,j}^k = 0, j \geq s_v + 1. \tag{41}$$

The initial conditions of the truck fleet are given by

$$X_{i,j}^1 = 0, \tag{42}$$

$$Y_{v,j}^1 = 0, v = \mathcal{V}/\{di\}, \tag{43}$$

$$Y_{di,j}^1 = m. \tag{44}$$

The following energy balance equation for year k holds

$$\sum_{j=1}^{s_{pv}} X_{pv,j}^k w_j^{pv} + \sum_{j=1}^{s_{wd}} X_{wd,j}^k w_j^{pv} + X_{grid}^k = W_{ba} \sum_{j=1}^{s_{ba}} Y_{ba,j}^k + W_e^{da} \sum_{j=1}^{s_{da}} X_{da,j}^k. \tag{45}$$

The net emission of the mining truck fleet in year k is given by

$$E^k = e_{di} \sum_{j=1}^{s_{di}} Y_{di,j}^k + e_n W_n^{da} \sum_{j=1}^{s_{da}} X_{da,j}^k + e_g X_{grid}^k - E_{ct}^k - E_{cc}^k, \tag{46}$$

where E_{ct}^k represent the trading amount of CO_2 in the year k and E_{cc}^k represent the amount of captured CO_2 in the year k.

The trading amount of CO_2 is limited by

$$E_{ct}^k \le \max\left\{ e_{di} \sum_{j=1}^{s_{di}} Y_{di,j}^k + e_g X_{grid}^k - E_{cc}^k, 0 \right\}. \tag{47}$$

To linearise the nonlinear constraint (47), a new binary decision variable z^k is introduced. Then, constraint (47) can be converted to constraints (48)–(51).

$$e_{di} \sum_{j=1}^{s_{di}} Y_{di,j}^k + e_g X_{grid}^k \ge E_{cc}^k - M(1 - z^k), \tag{48}$$

$$e_{di} \sum_{j=1}^{s_{di}} Y_{di,j}^k + e_g X_{grid}^k \le E_{cc}^k + M z^k, \tag{49}$$

$$E_{ct}^k \le e_{di} \sum_{j=1}^{s_{di}} Y_{di,j}^k + e_g X_{grid}^k - E_{cc}^k + M(1 - z^k), \tag{50}$$

$$E_{ct}^k \le 0 + M z^k. \tag{51}$$

To ensure that the converted constraints (48)–(51) are equivalent to the original constraints (47), a large positive constant M that is greater than or equal to the potential maximum value of the decision variables involved in the constraint should be selected.

The decarbonisation target can be written as

$$\sum_{k=1}^{K_h} E^k = 0, \tag{52}$$

The budget limit in year k is given as

$$\sum_{i=1}^{\mathcal{I}} c_{i,j}^{\mathcal{I},k} X_{i,j}^k + \sum_{v=1}^{\mathcal{V}} c_{v,j}^{\mathcal{V},k} Y_{v,j}^k + \sum_{i}^{\mathcal{I}} \sum_{j=1}^{s_i} l_i X_{i,j}^k + c_{ct}^k E_{ct}^k + c_{tax}^k u^k + c_{grid}^k X_{grid}^k \le B^k. \tag{53}$$

5. Case study

This section presents a case study for the decarbonisation planning of a truck fleet in a coal mine in Limpopo, South Africa. The coal mine is open-pit and uses conventional truck and shovel operation to produce coal products including thermal, metallurgical, and semi-soft coking coals. The mining right covers some 26 325 hectares. The annual production is 26.1 million tons. Currently, the mining truck fleet contains 27 diesel-powered mining trucks. The mining truck fleet is controlled by a vehicle dispatching system. Once the mine truck receives a dispatching order, it will travel to the assigned shovel. After that, the coal is loaded onto the truck and the truck hauls the material to the dump point. The truck is idling while waiting for a new dispatching order. This procedure is repeated until the end of the shift. The tramming capacity of trucks is 232 tons. The expected service life of mining trucks and utility vehicles is 10 years. Since the usage times of trucks are unknown, we assume the usage times of current mining trucks follow a uniform distribution from 1 to 10 years.

The numerical simulation is performed by using Gurobi solver [74], on an Intel Core i9-12900 CPU @3.20 GHz, 32 GB RAM. The solver uses the branch-and-cut algorithm to solve the obtained mix-integer programming problem. The termination condition for the branch-and-cut algorithm specifies that the difference between the lower and upper objective bounds is set to be less than 10^{-4}. The run time is 0.135 s. The simulation duration is from 2024 to 2050. The discount rate r is 8%. The prices of diesel-, battery-, and hydrogen-powered mining trucks are \$ 165 000, \$ 816 000, and \$ 386 000, respectively [75]. The salvage value is assumed to be 20% of the purchased price. The O&M cost is 5% of the purchase cost. The diesel and electricity prices in South Africa from 2011–2021 are obtained from the Department of Energy, South Africa [76,77], which are plotted in Fig. 8. Linear models are employed to fit the trends of diesel and electricity prices and predict their prices from 2024 to 2050. Since there is no mature green hydrogen market in South Africa currently and the historical green hydrogen price data is not available, the green hydrogen price from 2024 to 2050 is based on the prediction in [78]. The land cost is set to be 100 000 \$/km^2 per year.

The carbon tax has been implemented in many countries. The tax rate data is available in [72]. In South Africa, the Carbon Tax Act of 2019 came into effect on 1 June 2019. The first phase has a carbon tax rate of \$ 6.32 per ton of carbon dioxide equivalent emissions. This rate will increase annually by inflation plus 2% until 2025, and annually by inflation thereafter [79].

The levelised costs of energy (LCoE) for PV and wind power generation are calculated as

$$\text{LCoE} = \frac{\sum_{t=1}^{n} \frac{I_t + M_t}{(1+r)^2}}{\sum_{t=1}^{n} \frac{E_t}{(1+r)^2}}, \tag{54}$$

where I_t is the investment expenditures in the year t, M_t is the operations and maintenance expenditures in the year t, E_t is the electrical energy generated in the year t, and n is the expected lifetime of PV and wind turbine. The results are shown in Fig. 9. It can be observed that the LCoE of both PV and onshore wind energy in the area where the mine is located is lower than the LCoE of the grid electricity from 2031 and 2037, respectively. The potential of solar power generation in the location of the coal mine is higher than that of the onshore wind power generation.

The total costs of ownership (TCO) for trucks with different alternative power sources are calculated by

$$\text{TCO} = \text{Acquisition cost} + \text{O\&M costs} - \text{Salvage value}. \tag{55}$$

As shown in Fig. 10, the TCO of diesel-powered trucks is much higher BETs from 2024 to 2050. The TCOs of diesel-powered trucks and BETs using grid electricity increase fast from 2024 to 2050 due to the

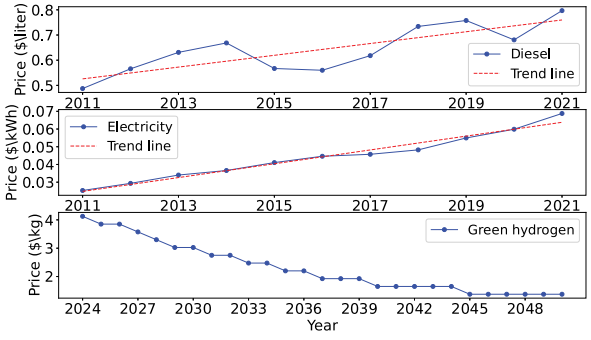


Fig. 8. Fuel and energy prices in South Africa.

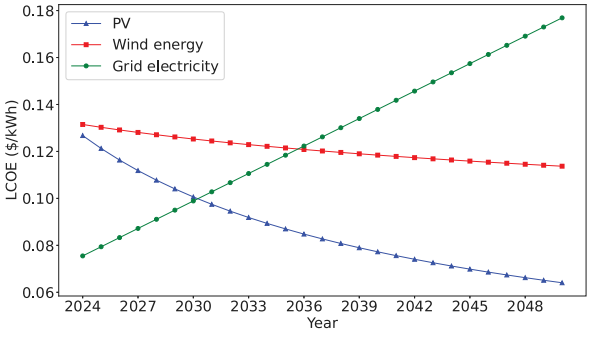


Fig. 9. LCoE of PV and wind power generation from 2024–2050.

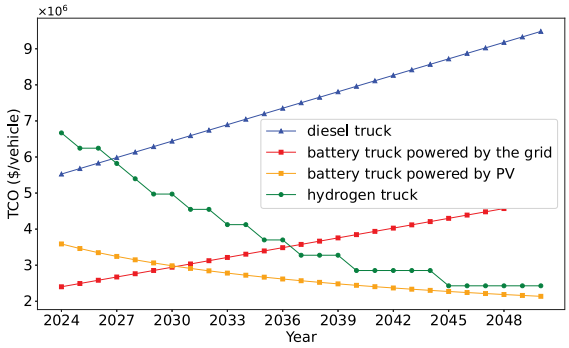


Fig. 10. TCO of trucks with alternative power sources from 2024 to 2050.

increase in diesel and grid electricity prices. The increase rate of TCO of diesel-powered trucks is higher than that of BETs using grid electricity. The TCOs of HFCTs and BETs using renewable energy decrease from 2024 to 2050. The TCO of BETs using renewable energy starts lower than the TCO of BETs using grid electricity from 2031. The TCO of green hydrogen-powered HFCTs starts lower than the TCO of BETs using grid electricity from 2037.

The levelised cost of carbon reduction (LCoC) for carbon capture technologies during 2024–2050 is calculated as

$$\mathrm{LCoC} = \frac{\sum_{i=t}^{n} \frac{I_t + M_t}{(1+r)^2}}{\sum_{t=1}^{n} \frac{C_t}{(1+r)^2}}, \tag{56}$$

where C_t is the amount of CO_2 captured in the year t. The LCoC of forestation, microalgae, and DAC using grid electricity and PV power generation are shown in Fig. 11. The LCoC of DAC supported by grid electricity keeps increasing due to the increase in grid electricity price, $ 532 $/ton in 2050. Although the LCoC of microalgae and DAC supported by PV power generation keep decreasing, 167 $/ton and 235 $/ton in 2050, respectively, forestation remains the least expensive carbon capture method for truck fleets (76 $/ton). It should be noted that forestation is sensitive to the land cost. When the land cost increases by 100%, the LCoC of forestation increases by 74% (135 $/ton), while the LCoC of microalgae in 2050 increases by 4% (176 $/ton).

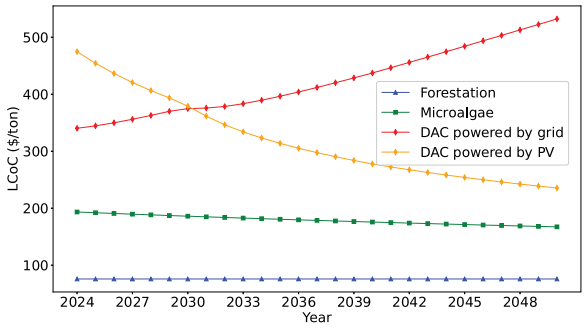
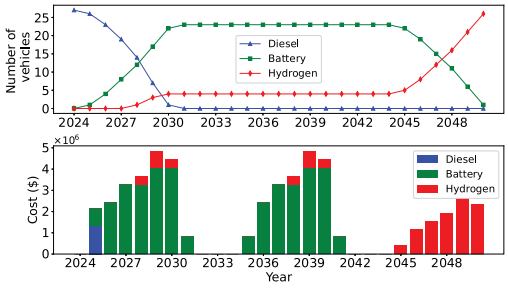


Fig. 11. LCoC of carbon capture technologies from 2024 to 2050.

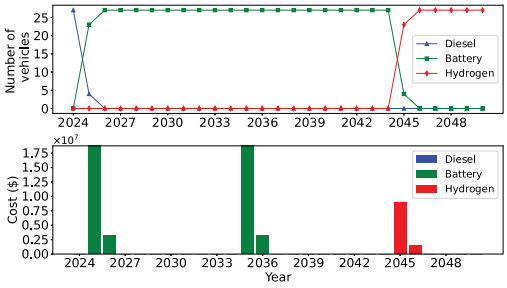
Since the annual budget has a significant impact on the decarbonisation pathway, two optimal decarbonisation pathways under different budget levels: low annual budget ($ 18 million) and high annual budget ($ 30 million) are shown in Figs. 12, including the annual investment plan for different types of trucks, renewable energy power generation, carbon capture technologies, and annual emissions for each scenario. The optimal LCCs under low and high annual budgets are $ 142 826 721 and $ 127 469 000, respectively. Both pathways involve investment in PV power generation, BET, HFCT, and forestation. According to Fig. 12(b), it is suggested to retire existing diesel-powered trucks as soon as possible under the high annual budget. Under the low annual budget, diesel-powered trucks can be selected before 2024 as shown in Fig. 12(a). The energy and fuel costs for diesel-, battery-, and HFCTs in 2024 are calculated as $ 1 226 367, $ 404 861, and $ 995 058, respectively. BETs are the first option to replace diesel-powered trucks before 2044. Under the low annual budget, HFCT can be a supplementary because its purchasing price is lower than BET. After 2044, HFCTs become the first choice of alternatives due to the decrease in the price of green hydrogen. As Fig. 12(d) shows, the installation of PV panels is expected to coincide with the adoption of BETs under the high annual budget. Under the low annual budget, the installation of PV panels has to be delayed as shown in Fig. 12(c). Due to the adoption of HCFTs after 2044, the planned capacity of PV decreases, which is caused by two reasons. One is the installed PV panels achieve service life. Another is actively retiring PV panels to save O&M costs when there are no battery trucks in the fleet. The actively retired capacity of PV under the low annual budget is significantly greater than that for the high annual budget. There are no more PV panels installed after 2044 because of the adoption of HFCTs. The forestation starts from 2044 under both low and high budgets to recycle the historical CO_2 emissions. Figs. 12(g) and 12(h) show the annual emission of the mining truck fleet for the two scenarios. The baseline emission of the truck fleet is computed based on the assumption that no investments will be made in decarbonisation technologies from 2024 to 2050. The annual emissions from 2026 to 2028 under the low annual budget and in 2025 under the high annual budget are greater than the baseline emissions due to the use of grid electricity, which demonstrates that electrification will increase the carbon emission of truck fleets in South Africa if they are powered by the grid. The truck fleet emits more CO_2 under the low annual budget than that under the high annual budget, 357 960 tons and 126 248 tons, respectively. Therefore, a higher level of forestation is required for the recycling of historical CO_2 emissions.

In the proposed models for truck energy consumption and carbon emissions, the correlation between annual miles and the energy consumption, as well as carbon emission of individual trucks, is simplified as linear. Given that the annual miles of the trucks are estimated, a sensitivity analysis is conducted to elucidate the impact of annual mileage uncertainty on the optimal decarbonisation pathway. Three scenarios are considered: the base scenario (denoted as M), an increase in annual mileage by 10% (denoted as 110%M), and a decrease in annual mileage by 10% (denoted as 90%M). The high annual budget ($ 30 million) is applied. Fig. 13 illustrates the planned number of various truck types, the planned capacity of PV power generation, and the planned forestation area. Simulation results indicate that the uncertainty in annual miles does not influence the selection of decarbonisation technologies of the optimal decarbonisation pathway but does impact their planned capacity. Lower annual mileage results in reduced annual fuel costs, enabling more timely replacement of diesel trucks with BETs within the limited annual budget. Consequently, Fig. 13(a) reveals that in 2025, the 90%M scenario sees more diesel-powered trucks being replaced by BETs. With lower annual mileage, there are correspondingly lower planned capacities for PV power generation and forestation areas. In contrast to the base scenario (M) with an optimal LCC of $ 127 469 000, the optimal LCCs for the 90%M and 110%M scenarios are $ 121 076 771, $ 133 925 000, respectively. This represents a decrease of 5% in LCC for the 90%M scenario and an increase of 5% in LCC for the 110%M scenario compared to the base scenario.

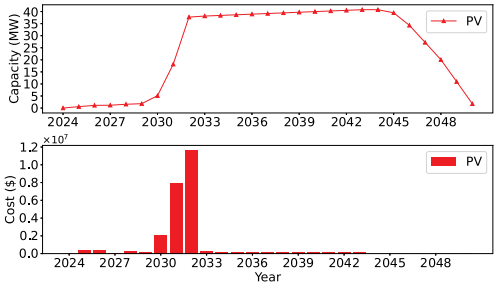
Our study examines the influence of carbon trading prices on the optimal decarbonisation pathway. Using the three carbon price models outlined in Table 3, we present simulation results in Fig. 14. The optimal LCCs under low, middle, and high carbon trading price scenarios



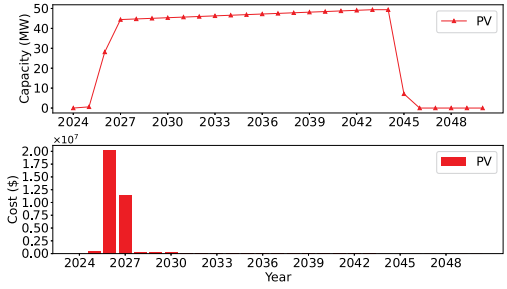
(a) The planned number of trucks and annual investment cost under low annual budget.



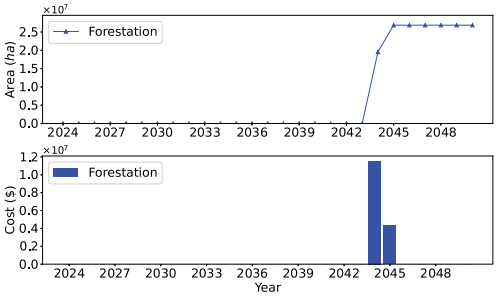
(b) The planned number of trucks and investment cost under high annual budget.



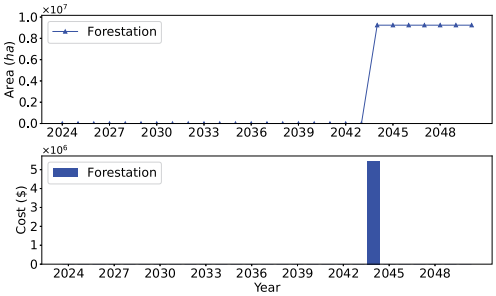
(c) The planned capacity and annual investment cost of PV power generation under low annual budget.



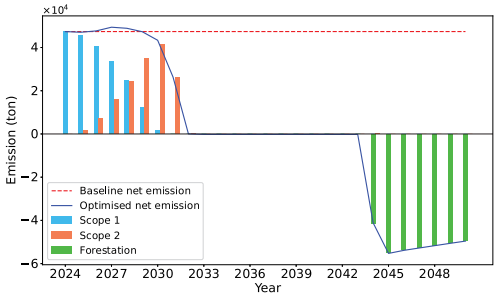
(d) The planned number of trucks and investment cost under high annual budget.



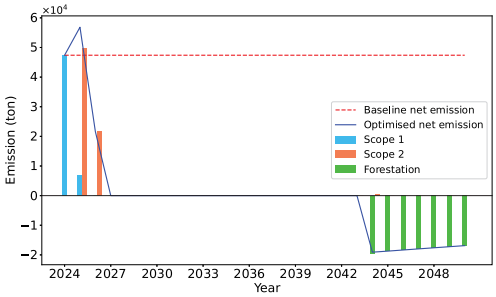
(e) The planned capacity and annual investment cost of carbon capture technologies under low annual budget.



(f) The planned capacity and annual investment cost of carbon capture technologies under high annual budget.

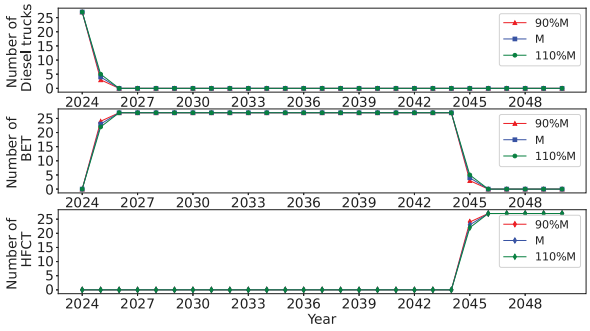


(g) The annual emissions under low annual budget.

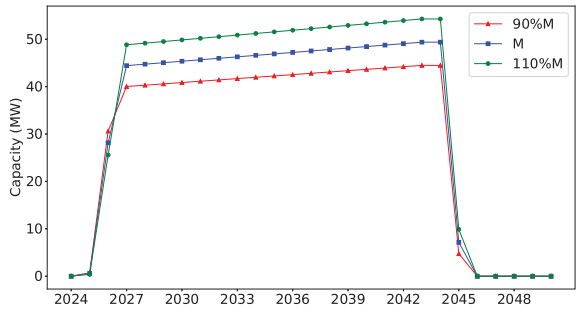


(h) The annual emissions under high annual budget.

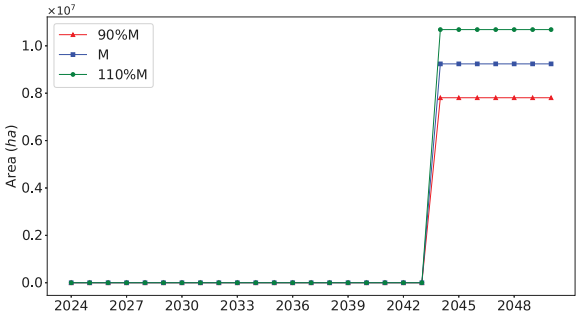
Fig. 12. The optimal decarbonisation pathways under low and high annual budgets.



(a) The planned number of different types of trucks.



(b) The planned capacity of PV power generation.



(c) The planned capacity of forestation.

Fig. 13. The optimal decarbonisation pathways with different annual mileage of trucks.

are $ 135 135 981, $ 135 808 793, and $ 13 720 937, respectively. We observe that the optimal decarbonisation pathways under both low and middle carbon price scenarios are similar. Theoretically, higher trading prices facilitate a more rapid transition from diesel-powered trucks to BETs. However, when there is a budget limit, higher annual carbon trading cost delays the replacement of diesel-powered trucks, evident in the numbers of diesel-powered trucks in the year 2029 as depicted in Figs. 12(c) and 14(c). Specifically, In 2029, under the low and middle carbon price scenarios, there are still one and two diesel-powered trucks in the fleet, respectively. The corresponding annual costs for 2029 are $ 17 320 018 and $ 17 315 875, respectively, nearly approaching the annual budget of $ 18 000 000. Importantly, these findings suggest that when carbon trading prices are too low, achieving the decarbonisation target for the mining truck fleet can be directly realised through carbon trading. From a policymaker's perspective, this implies that low carbon trading prices may not effectively incentivise the mining industry to actively invest in carbon capture technology. The results under high carbon trading price scenario underscore this point. Under the high carbon trading prices, afforestation becomes a viable option for carbon capture, expanding the range of strategies beyond solely relying on carbon trading.

6. Conclusion

In this study, the optimal decarbonisation pathway for mining truck fleets is investigated. The technical, financial, and environmental performance of multiple decarbonisation technologies, including mining trucks with alternative power sources, renewable power generations, carbon capture technologies, and carbon trading are investigated. A mix-integer programming model is built to determine the annual investment combination of different carbon reduction technologies under the carbon neutrality target. A case study for the optimal decarbonisation pathway of truck fleets in a South African coal mine is conducted to illustrate the proposed method. The identified optimal pathway outlines an investment plan encompassing PV, BET, HFCT, and forestation. It suggests replacing current diesel-powered trucks with BETs and deploying PV infrastructure to support BET charging as soon as possible if the budget allows. HFCTs become more cost-effective compared to BETs after 2044. Forestation is regarded as the most cost-effective way among carbon capture technologies. In addition, the prevailing carbon trading prices enable the truck fleet to achieve decarbonisation solely through carbon trading without necessitating investment in specific carbon capture technologies. The proposed method guides the decarbonisation of the mining transportation fleet and provides a research basis for the decarbonisation of the entire mine industry.

CRediT authorship contribution statement

Gang Yu: Writing – original draft. **Xianming Ye:** Writing – review & editing, Supervision, Funding acquisition, Formal analysis. **Yuxiang Ye:** Writing – review & editing, Formal analysis. **Hongxu Huang:** Conceptualization. **Xiaohua Xia:** Supervision, Funding acquisition.

Declaration of competing interest

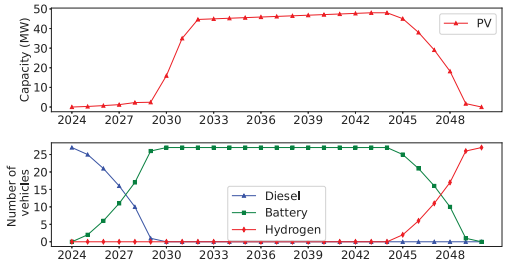
The authors declare the following financial interests/personal relationships which may be considered as potential competing interests: Xianming Ye reports financial support was provided by Royal Academy of Engineering. Xianming Ye reports financial support was provided by National Research Foundation. Xiaohua Xia is an Advisory Board Member for *Journal of Automation and Intelligence* and was not involved in the editorial review or the decision to publish this article. If there are other authors, they declare that they have no known competing financial interests or personal relationships that could have appeared to influence the work reported in this paper.

Data availability

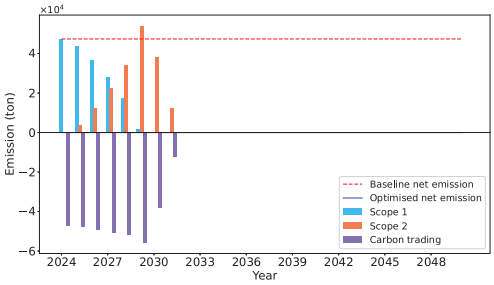
Data will be made available on request.

Acknowledgements

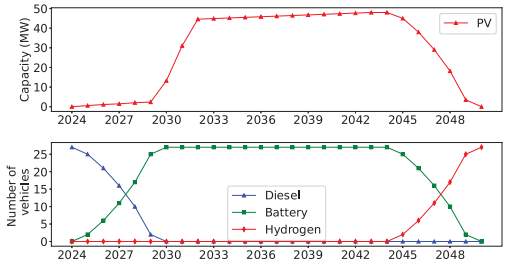
This research is jointly supported by National Key R&D Program of China (Grant No. 2021YFE0199000), National Natural Science Foundation of China (Grant No. 62133015), National Research Foundation China/South Africa Research Cooperation Programme with Grant No. 148762, and Royal Academy of Engineering Transforming Systems through Partnership grant scheme with reference No. TSP2021\100016.



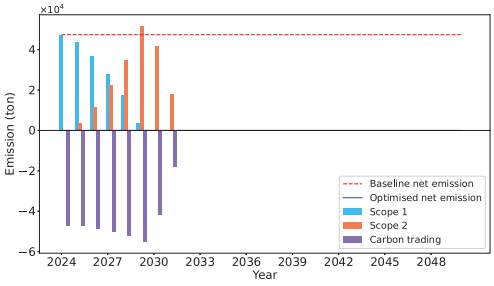
(a) The planned capacity of PV and number of trucks under low trading price scenario.



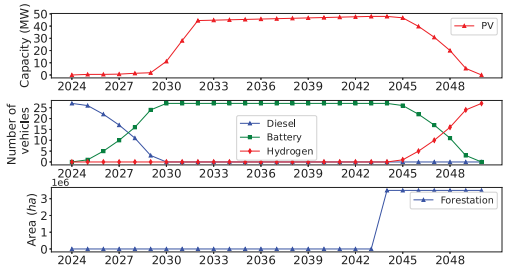
(b) Annual emissions under low trading price scenario.



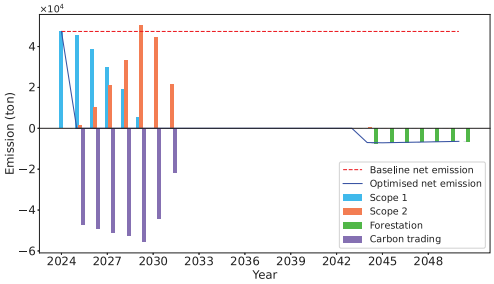
(c) The planned capacity of PV and number of trucks under middle trading price scenario.



(d) Annual emissions under middle trading price scenario.



(e) The planned capacity of PV and number of trucks under high trading price scenario.



(f) Annual emissions under high trading price scenario.

Fig. 14. The optimal decarbonisation pathways under low, middle, and high carbon trading price scenarios.

References

[1] L. Henry, M.F. Clemens, N. Tomas, O. Erik, Creating the zero-carbon mine, Technical Report, McKinsey, 2021.

[2] T.D. Pearce, J.D. Ford, J. Prno, F. Duerden, J. Pittman, M. Beaumier, L. Berrang-Ford, B. Smit, Climate change and mining in Canada, in: Mitigation and Adaptation Strategies for Global Change, vol. 16, Springer, 2011, pp. 347–368.

[3] J. Phillips, Climate change and surface mining: A review of environment-human interactions & their spatial dynamics, Appl. Geogr. 74 (2016) 95–108.

[4] D. Meza-Figueroa, R.M. Maier, M. de la O-Villanueva, A. Gómez-Álvarez, A. Moreno-Zazueta, J. Rivera, A. Campillo, C.J. Grandlic, R. Anaya, J. Palafox-Reyes, The impact of unconfined mine tailings in residential areas from a mining town in a semi-arid environment: Nacozari, Sonora, Mexico, Chemosphere 77 (1) (2009) 140–147.

[5] G.B. Simpson, J. Badenhorst, G.P. Jewitt, M. Berchner, E. Davies, Competition for land: the water-energy-food nexus and coal mining in Mpumalanga Province, South Africa, Front. Environ. Sci. 7 (2019) 86.

[6] M. Bobotis, On the path to zero emissions: how the mining industry is working towards GHG-free surface mining, 2021, https://www.hatch.com/About-Us/Publications/Blogs/2021/05/On-the-path-to-zero-emissions. (Accessed 11 April 2024).

[7] Y. Feng, Q. Liu, Y. Li, J. Yang, Z. Dong, Energy efficiency and CO_2 emission comparison of alternative powertrain solutions for mining haul truck using integrated design and control optimization, J. Clean. Prod. 370 (2022) 133568.

[8] J.H. Williams, R.A. Jones, B. Haley, G. Kwok, J. Hargreaves, J. Farbes, M.S. Torn, Carbon-neutral pathways for the United States, AGU Adv. 2 (1) (2021) e2020AV000284.

[9] Standard, GHG Protocol, The greenhouse gas protocol, 2011.

[10] UNFCCC, The Paris agreement, 2015, https://www.ipcc.ch/sr15/. (Accessed 11 April 2024).

[11] C.A. Romero, P. Correa, E.A. Ariza Echeverri, D. Vergara, Strategies for reducing automobile fuel consumption, Appl. Sci. 14 (2) (2024) 910.

[12] D. Huo, Y.A. Sari, Q. Zhang, Smart dispatching for low-carbon mining fleet: A deep reinforcement learning approach, J. Clean. Prod. (2024) 140459.

[13] C. De Saxe, J. van Eeden, L. Kemp, A. Steenkamp, J. Cowper, High-capacity coal trucks to reduce costs and emissions at South Africa's power utility, Res. Transp. Bus. Manag. (2022) 100898.

[14] M.J. Haugen, L. Paoli, J. Cullen, D. Cebon, A.M. Boies, A fork in the road: Which energy pathway offers the greatest energy efficiency and CO_2 reduction potential for low-carbon vehicles? Appl. Energy 283 (2021) 116295.

[15] B. Sen, T. Ercan, O. Tatari, Does a battery-electric truck make a difference?–Life cycle emissions, costs, and externality analysis of alternative fuel-powered Class 8 heavy-duty trucks in the United States, J. Clean. Prod. 141 (2017) 110–121.

[16] L.W. Yeow, Y. Yan, L. Cheah, Life cycle greenhouse gas emissions of alternative fuels and powertrains for medium-duty trucks: A Singapore case study, Transp. Res. D 105 (2022) 103258.

[17] S. Pelletier, O. Jabali, J.E. Mendoza, G. Laporte, The electric bus fleet transition problem, Transp. Res. C 109 (2019) 174–193.

[18] O.C. Campo, R.Á. Fernández, Economic optimization analysis of different electric powertrain technologies for vans applied to last mile delivery fleets, J. Clean. Prod. 385 (2023) 135677.

[19] O. Alp, T. Tan, M. Udenio, Transitioning to sustainable freight transportation by integrating fleet replacement and charging infrastructure decisions, Omega 109 (2022) 102595.

[20] V. Balboa-Espinoza, J. Segura-Salazar, C. Hunt, D. Aitken, L. Campos, Comparative life cycle assessment of battery-electric and diesel underground mining trucks, J. Clean. Prod. 425 (2023) 139056.

[21] N. Nwankwo, T.K. Olaniyi, A. Morgan, A just transition framework for oil rich Sub-Saharan Africa countries, Int. J. Sustain. Energy 11 (1) (2023).

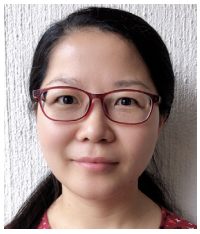
[22] W.L. Theo, J.S. Lim, H. Hashim, A.A. Mustaffa, W.S. Ho, Review of pre-combustion capture and ionic liquid in carbon capture and storage, Appl. Energy 183 (2016) 1633–1663.
[23] M. Tatsumi, Y. Yagi, K. Kadono, K. Kaibara, M. Iijima, T. Ohishi, H. Tanaka, T. Hirata, R. Mitchell, New energy efficient processes and improvements for flue gas CO_2 capture, Energy Procedia 4 (2011) 1347–1352.
[24] Global CCS Institute, Projects database: Large-scale CCS facilities, Global CCS Institute Melbourne, 2017.
[25] K. Goto, K. Yogo, T. Higashii, A review of efficiency penalty in a coal-fired power plant with post-combustion CO_2 capture, Appl. Energy 111 (2013) 710–720.
[26] K.T. Vashum, S. Jayakumar, Methods to estimate above-ground biomass and carbon stock in natural forests-a review, J. Ecosyst. Ecograph. 2 (4) (2012) 1–7.
[27] M.N. Högberg, M.J. Briones, S.G. Keel, D.B. Metcalfe, C. Campbell, A.J. Midwood, B. Thornton, V. Hurry, S. Linder, T. Näsholm, et al., Quantification of effects of season and nitrogen supply on tree below-ground carbon transfer to ectomycorrhizal fungi and other soil organisms in a boreal pine forest, New Phytol. 187 (2) (2010) 485–493.
[28] E. Marín-Spiotta, S. Sharma, Carbon storage in successional and plantation forest soils: a tropical analysis, Global Ecol. Biogeogr. 22 (1) (2013) 105–117.
[29] J. Ge, Z.J. Zhang, B. Lin, Towards carbon neutrality: How much do forest carbon sinks cost in China? Environ. Impact Assess. Rev. 98 (2023) 106949.
[30] L. Mo, C.M. Zohner, P.B. Reich, J. Liang, S. De Miguel, G.J. Nabuurs, S.S. Renner, J. van den Hoogen, A. Araza, M. Herold, et al., Integrated global assessment of the natural forest carbon potential, Nature (2023) 1–10.
[31] H. Onyeaka, T. Miri, K. Obileke, A. Hart, C. Anumudu, Z.T. Al-Sharify, Minimizing carbon footprint via microalgae as a biological capture, Carbon Capt. Sci. Technol. 1 (2021) 100007.
[32] W.Y. Cheah, T.C. Ling, J.C. Juan, D.J. Lee, J.S. Chang, P.L. Show, Biorefineries of carbon dioxide: From carbon capture and storage (CCS) to bioenergies production, Bioresour. Technol. 215 (2016) 346–356.
[33] G. Yadav, S.K. Dash, R. Sen, A biorefinery for valorization of industrial waste-water and flue gas by microalgae for waste mitigation, carbon-dioxide sequestration and algal biomass production, Sci. Total Environ. 688 (2019) 129–135.
[34] M. Erans, E.S. Sanz-Pérez, D.P. Hanak, Z. Clulow, D.M. Reiner, G.A. Mutch, Direct air capture: process technology, techno-economic and socio-political challenges, Energy Environ. Sci. 15 (4) (2022) 1360–1405.
[35] L. Jiang, W. Liu, R. Wang, A. Gonzalez-Diaz, M. Rojas-Michaga, S. Michailos, M. Pourkashanian, X. Zhang, C. Font-Palma, Sorption direct air capture with CO_2 utilization, Prog. Energy Combust. Sci. 95 (2023) 101069.
[36] H. Azarabadi, K.S. Lackner, A sorbent-focused techno-economic analysis of direct air capture, Appl. Energy 250 (2019) 959–975.
[37] O.O. Ayeleru, H.U. Modekwe, O.R. Onisuru, C.R. Ohoro, C.A. Akinnawo, P.A. Olubambi, Adsorbent technologies and applications for carbon capture, and direct air capture in environmental perspective and sustainable climate action, Sustain. Chem. Clim. Action (2023) 100029.
[38] J. Rogelj, M. Schaeffer, M. Meinshausen, R. Knutti, J. Alcamo, K. Riahi, W. Hare, Zero emission targets as long-term global goals for climate protection, Environ. Res. Lett. 10 (10) (2015) 105007.
[39] M.A. Pourmoosavi, T. Amraee, Low carbon generation expansion planning with carbon capture technology and coal phase-out under renewable integration, Int. J. Electr. Power Energy Syst. 128 (2021) 106715.
[40] E.G. Hertwich, R. Wood, The growing importance of Scope 3 greenhouse gas emissions from industry, Environ. Res. Lett. 13 (10) (2018) 104013.
[41] S. Eggleston, L. Buendia, K. Miwa, T. Ngara, K. Tanabe, 2006 IPCC guidelines for national greenhouse gas inventories. Volume 1. General guidance and reporting, Inst. Glob. Environ. Strateg. (IGES) (2006).
[42] L.K. Sahoo, S. Bandyopadhyay, R. Banerjee, Benchmarking energy consumption for dump trucks in mines, Appl. Energy 113 (2014) 1382–1396.
[43] A. Lajunen, Fuel economy analysis of conventional and hybrid heavy vehicle combinations over real-world operating routes, Transp. Res. D 31 (2014) 70–84.
[44] W. Yang, J. Liang, J. Yang, N. Zhang, Investigation of a novel coaxial power-split hybrid powertrain for mining trucks, Energies 11 (1) (2018) 172.
[45] NASA, The POWER Project, 2023, https://power.larc.nasa.gov/. (Accessed 11 April 2024).
[46] IEA, Solar PV, 2022, https://www.iea.org/reports/solar-pv. (Accessed 11 April 2024).
[47] C. Ballif, F.J. Haug, M. Boccard, P.J. Verlinden, G. Hahn, Status and perspectives of crystalline silicon photovoltaics in research and industry, Nat. Rev. Mater. 7 (8) (2022) 597–616.
[48] M. Senatla, R.C. Bansal, R. Naidoo, L. Chiloane, U. Mudau, Estimating the economic potential of PV rooftop systems in South Africa's residential sector: a tale of eight metropolitan cities, IET Renew. Power Gener. 14 (4) (2020) 506–514.
[49] S.C. Pryor, R.J. Barthelmie, M.S. Bukovsky, L.R. Leung, K. Sakaguchi, Climate change impacts on wind power generation, Nat. Rev. Earth Environ. 1 (12) (2020) 627–643.
[50] E. Alsema, M.J. De Wild, Environmental impact of crystalline silicon photovoltaic module production, MRS Online Proc. Libr. 895 (2005) 0895–G03.
[51] L.E. Yelle, The learning curve: Historical review and comprehensive survey, Decis. Sci. 10 (2) (1979) 302–328.
[52] M. Grubb, P. Drummond, A. Poncia, W. McDowall, D. Popp, S. Samadi, C. Penasco, K.T. Gillingham, S. Smulders, M. Glachant, et al., Induced innovation in energy technologies and systems: a review of evidence and potential implications for CO_2 mitigation, Environ. Res. Lett. 16 (4) (2021) 043007.
[53] International Renewable Energy Agency (IRENA), Renewable power generation costs in 2022, Technical Report, International Renewable Energy Agency, 2022.
[54] International Renewable Energy Agency, Renewable Capacity Statistics 2023, Technical Report, International Renewable Energy Agency (IRENA), 2023.
[55] D. Lefebvre, A.G. Williams, G.J. Kirk, J. Burgess, J. Meersmans, M.R. Silman, F. Román-Dañobeytia, J. Farfan, P. Smith, Assessing the carbon capture potential of a reforestation project, Sci. Rep. 11 (1) (2021) 19907.
[56] J. Sullivan, G.S. Amacher, Optimal hardwood tree planting and forest reclamation policy on reclaimed surface mine lands in the Appalachian coal region, Resour. Policy 38 (1) (2013) 1–7.
[57] S.K. Jayaraman, R.R. Rhinehart, Modeling and optimization of algae growth, Ind. Eng. Chem. Res. 54 (33) (2015) 8063–8071.
[58] E. Lee, M. Jalalizadeh, Q. Zhang, Growth kinetic models for microalgae cultivation: A review, Algal Res. 12 (2015) 497–512.
[59] Q. Béchet, A. Shilton, B. Guieysse, Modeling the effects of light and temperature on algae growth: state of the art and critical assessment for productivity prediction during outdoor cultivation, Biotech. Adv. 31 (8) (2013) 1648–1663.
[60] J.M. Greene, D. Quiroz, S. Compton, P.J. Lammers, J.C. Quinn, A validated thermal and biological model for predicting algal productivity in large scale outdoor cultivation systems, Algal Res. 54 (2021) 102224.
[61] M. Marsullo, A. Mian, A.V. Ensinas, G. Manente, A. Lazzaretto, F. Marechal, Dynamic modeling of the microalgae cultivation phase for energy production in open raceway ponds and flat panel photobioreactors, Front. Energy Res. 3 (2015) 41.
[62] M. Tsubo, S. Walker, Relationships between photosynthetically active radiation and clearness index at Bloemfontein, South Africa, Theor. Appl. Climatol. 80 (2005) 17–25.
[63] A. Yang, Modeling and evaluation of CO_2 supply and utilization in algal ponds, Ind. Eng. Chem. Res. 50 (19) (2011) 11181–11192.
[64] S. Yadala, S. Cremaschi, A dynamic optimization model for designing open-channel raceway ponds for batch production of algal biomass, Processes 4 (2) (2016) 10.
[65] B. Guieysse, Q. Béchet, A. Shilton, Variability and uncertainty in water demand and water footprint assessments of fresh algae cultivation based on case studies from five climatic regions, Bioresour. Technol. 128 (2013) 317–323.
[66] S. Banerjee, S. Ramaswamy, Comparison of productivity and economic analysis of microalgae cultivation in open raceways and flat panel photobioreactor, Bioresour. Technol. Rep. 8 (2019) 100328.
[67] D.H. Lee, Levelized cost of energy and financial evaluation for biobutanol, algal biodiesel and biohydrogen during commercial development, Int. J. Hydrogen Energy 41 (46) (2016) 21583–21599.
[68] Food and Agriculture Organization of the United Nations, Global Seaweeds and Microalgae Production, 1950–2019, Technical Report, United Nations, 2021.
[69] N. McQueen, M.J. Desmond, R.H. Socolow, P. Psarras, J. Wilcox, Natural gas vs. electricity for solvent-based direct air capture, Front. Clim. 2 (2021) 618644.
[70] International Energy Agency, Direct air capture: A key technology for net zero, Technical Report, International Energy Agency (IEA), 2022.
[71] M. Fasihi, O. Efimova, C. Breyer, Techno-economic assessment of CO_2 direct air capture plants, J. Clean. Prod. 224 (2019) 957–980.
[72] W. Bank, Carbon pricing dashboard, 2023, https://carbonpricingdashboard.worldbank.org/. (Accessed 11 April 2024).
[73] H. Kalantari, A.P. Sasmito, S.A. Ghoreishi-Madiseh, An overview of directions for decarbonization of energy systems in cold climate remote mines, Renew. Sustain. Energy Rev. 152 (2021) 111711.
[74] Gurobi, Gurobi optimization, 2023, https://www.gurobi.com/. (Accessed 11 April 2024).
[75] B. Sharpe, H. Basma, A meta-study of purchase costs for zero-emission trucks, Int. Counc. Clean Energy Transp. (s 18) (2022).
[76] Energy Statistics, Monthly fuel retail/pump prices, 2023, https://www.energy.gov.za/files/energyStats_frame.html. (Accessed 11 April 2024).
[77] Eskom, Tariff history, 2023, https://www.eskom.co.za/distribution/tariffs-and-charges/tariff-history/. (Accessed 11 April 2024).
[78] PwC, Green hydrogen economy - predicted development of tomorrow, 2020, https://www.pwc.com/gx/en/industries/energy-utilities-resources/future-energy/green-hydrogen-cost.html. (Accessed 11 April 2024).
[79] South African Revenue Service (SARS), Carbon tax, 2021, https://www.sars.gov.za/customs-and-excise/excise/environmental-levy-products/carbon-tax/. (Accessed 11 April 2024).



Gang Yu received the B.S. degree in automation from Wuhan University of Technology, China, in 2016, the M.S. degree in control theory and control engineering from China Three Gorges University, China, in 2020. He is currently working toward the Ph.D. degree in electrical engineering in University of Pretoria, South Africa. His research interests include the green transition of transportation system, energy management and optimisation.



Xianming Ye received his BEng and MEng degrees from the Department of Automation, Wuhan University, China, in 2008 and 2010, respectively. He completed his Ph.D. degree in Electrical Engineering from the University of Pretoria in 2015. He is currently an Associate Professor and the Junior Exxaro Chair in Energy Efficiency in the Department of Electrical, Electronic, and Computer Engineering at the University of Pretoria, South Africa. He is also a Certified Measurement and Verification Professional. His research interests include modelling and optimisation of energy systems in buildings and industries, renewable energy, microgrids, P2P energy sharing, battery management systems, explainable AI, and electric vehicles. He is a Guest Editor for IEEE Transactions on Consumer Electronics and an Associate Editor for IET Renewable Power Generation.



Yuxiang Ye obtained her Ph.D. degree in 2020 from the Department of Economics, University of Pretoria, South Africa. She is currently a Senior Lecturer in the School of Economics and Finance at the University of the Witwatersrand (Wits University), Johannesburg, South Africa. Her academic interests are mainly focused on Energy Economics, and Applied Microeconomics.



Hongxu Huang received the degree of B.Sc. Eng. in 2019 from China University of Mining and Technology, China, where he is currently working toward the Ph.D. degree in electrical engineering. From 2021 to 2022, He was a visiting Ph.D. student at Nanyang Technological University, Singapore. His research interests include optimisation under uncertainties and decentralised energy trading.



Xiaohua Xia (Fellow, IEEE) received his B.Sc. degree in Applied Mathematics from Wuhan Institute of Hydraulic and Electrical Engineering, Wuhan, China, in 1983 and the Ph.D. degree in Automatic Control Theory and Application from Beijing University of Aeronautics and Astronautics, Beijing, China, in 1989. He is currently a Professor in the Department of Electrical, Electronic, and Computer Engineering at the University of Pretoria, South Africa, Director of the Centre for New Energy Systems, and Director of the National Hub for the Postgraduate Programme in Energy Efficiency and Demand Side Management. He was academically affiliated with the University of Stuttgart, Stuttgart, Germany, the Ecole Centrale de Nantes, Nantes, France, and the National University of Singapore, Singapore, before joining the University of Pretoria, Pretoria, South Africa in 1998. His current research interests include industrial energy systems and building energy systems, etc. He is an IEEE fellow and an NRF A-rated scientist. He is a registered Professional Engineer with the Engineering Council of South Africa. He was elected a fellow of the South African Academy of Engineering in 2005, and a member of the Academy of Science of South Africa in 2011. He has been an Associate Editor of Automatica, IEEE Transactions on Circuits and Systems II, IEEE Transactions on Automatic Control, and Specialist Editor (Control) of the SAIEE Africa Research Journal, and currently sits on the editorial board of Applied Energy.